Dimer formation of GdDO3A-arylsulfonamide complexes causes loss of pH-dependency of relaxivity[i]

Anja Wacker[a], Fabio Carniato[b], Carlos Platas-Iglesias[c], David Esteban-Gómez[c], Hans-Jürgen Wester[a], Lorenzo Tei[b*] and Johannes Notni[a†]

[a] Lehrstuhl für Pharmazeutische Radiochemie, Technische Universität München, Walther-Meißner-Strasse 3, D-85748 Garching, Germany

[b] Dipartimento di Scienze e Innovazione Tecnologica, Università del Piemonte Orientale "Amedeo Avogadro", Viale T. Michel 11, I-15121 Alessandria, Italy

[c] Centro de Investigacións Científicas Avanzadas (CICA) and Departamento de Química Fundamental, Facultade de Ciencias, Universidade da Coruña, E-15071, A Coruña, Galicia, Spain

Dalton Transactions, volume 46, issue 48, pages 16828–16836, 28 December 2017
Submitted 11 August 2017, accepted 06 November 2017, first published 06 November 2017

How to cite:

A. Wacker, F. Carniato, C. Platas-Iglesias, D. Esteban-Gómez, H.-J. Wester, L. Tei and J. Notni, Dimer formation of GdDO3A-arylsulfonamide complexes causes loss of pH-dependency of relaxivity, *Dalt. Trans.*, 2017, **46**, 16828–16836. DOI: 10.1039/C7DT02985C.

Abstract

Gadolinium(III) complexes with pH-dependent relaxivities have been proposed as responsive magnetic resonance imaging (MRI) contrast agents (CA) for mapping of pH value in living subjects. The latter is clinically relevant because hypoxia-induced reduction of interstitial pH (acidosis) is a hallmark of tumor progression and resistance against chemotherapy. In order to obtain versatile building blocks for integration of a pH-responsive MRI-CA functionality into larger molecular assemblies, such as bioconjugates, micelles or nanoparticles, we equipped the structural motif GdDO3A-ethylene(arylsulfonic acid) with additional carboxylic acid moieties in the aromatic *para*-position. Two novel compounds were characterized concerning their pH-dependent relaxivity as well as by ^{17}O NMR and ^{1}H NMRD, augmented by determination of luminescence lifetimes of the respective Eu(III) complexes and structural modelling by density functional theory (TPSSh/LCRECP/6-31G(d)). Unexpected involvement of the peripheral carboxylates into metal ion complexation effected self-assembly of the lanthanide(III) complexes, resulting in dimeric species comprising two lanthanide ions, two symmetrically bridging ligands, and one coordinated water molecule per Gd(III) (q = 1). These structures are stable even at low concentrations and in presence of competing anions like phosphate. The pH-sensitive sulfonamide moieties are not involved into Gd(III) coordination, resulting in virtually constant relaxivities of r_1 = 6.7 $mM^{-1} s^{-1}$ (298 K, 20 MHz) over the biologically relevant pH range (4 to 9). Since further functionalisation on the peripheral carboxylates would effectively inhibit dimer formation, the compounds are nonetheless suited for the initially envisaged field of application.

* lorenzo.tei@uniupo.it
† johannes.notni@tum.de

Introduction

Magnetic resonance imaging (MRI) is a well-established, powerful tool in non-invasive routine clinical diagnostics. The most important advantages over computed tomography (CT) are absence of ionizing radiation and a superior soft tissue contrast.[1] Image contrast is derived from substantially different T_1 or T_2 proton relaxation times in various tissues. The contrast can further be enhanced by application of MRI contrast agents (CA), that is, compounds affecting proton relaxation, for example, strongly paramagnetic Gd^{III} complexes which reduce T_1 of protons in their vicinity. Moreover, the portfolio of MRI applications ranges beyond imaging of morphology. Noninvasive mapping of certain physiological parameters can be realized, for example, of tissue perfusion by means of special pulse sequences (arterial spin labeling, ASL) or using contrast agents (dynamic contrast enhanced MRI, DCE-MRI). MR imaging of complex biological functions can be achieved with even more sophisticated approaches, such as blood oxygenation level dependent (BOLD) contrast MRI[2] which exploits the natural differences in magnetic susceptibility of diamagnetic low-spin Fe^{II} and paramagnetic high-spin Fe^{II} in oxygenized and non-oxygenized haemoglobin,[3] respectively. It is primarily used for mapping of brain activity *via* measurement of neuronal oxygen consumption, a technique referred to as functional MRI (fMRI).[4]

From a chemical point of view, BOLD-contrast imaging perfectly showcases a powerful strategy in MRI-CA design. It utilizes the Fe^{II}–porphyrin complex haem as a naturally abundant CA whose relaxivity is dependent from, or responds to, an environmental parameter, namely, oxygen consumption. An entire class of artificial '(bio)responsive',[5] 'activatable',[6] or 'smart'[7] MRI-CA is essentially founded on the same idea. Many of these approaches are based on Gd^{III} complexes[8] whose relaxivity is modulated by changes in environmental pH, oxygen partial pressure,[9] enzyme activity,[10] or the presence of other metal cations.[11] Therefore, they can 'report' changes in their physical or chemical environment and are thus, in principle, useful for high-resolution 3D-mapping of said parameters by MRI systems.

On a molecular level, said modulation of relaxivity is usually a result of a parameter-dependent change of structural features of the Gd^{III} complex, affecting the mode of interaction and magnetic coupling between the paramagnetic Gd^{III} ion and the surrounding water molecules, for example, the number of Gd^{III}-coordinated 'inner-sphere' water molecules q, their exchange lifetime τ_M, or the reorientational correlation time or 'tumbling speed' τ_R. In terms of pH-sensitive CA, the first reported example was a Gd^{III} complex of the tetraphosphonate-DOTAM derivative Gd-DOTA-4Amp.[12] For this complex, a variation of pH modulates its relaxivity by changing the protonation state of the pendant phosphonates which, in turn, affects τ_M by altering the exchange rate of relaxed water protons with protons of the bulk.[13] In contrast, pH-dependency of the relaxivity of Gd-DO3A complexes with one β-sulfonamidoethyl pendant arm (GdDO3A-SA)[14–16] is rooted in a pH-dependent number of Gd^{III}-bound aqua ligands q. While at acidic pH, the sulfonamide is *N*-protonated and thus unable to bind to Gd^{III}, leaving room for more than one aqua ligand ($q \sim 2$) at the metal centre, coordination of the deprotonated sulfonamide nitrogen at pH > 7 replaces all Gd-bound water, resulting in $q = 0$ and thus, a markedly lower relaxivity ($\Delta r_1 \sim 5.5\ mM^{-1}\ s^{-1}$). Such GdDO3A-SA-like complexes have been modified to bind to HSA[17] or encapsulated in liposomes[18] aiming to further increase the extent of pH-dependent variation of relaxivity. The corresponding EuDO3A-SA complexes have been decorated with photosensitizers, and the resulting constructs were successfully applied for measurement of changes of intracellular pH, *e.g.*, in lysosomes or the endoplasmic reticulum.[19] Structurally related Ln-DO3A systems, featuring aminoethyl or diphenylphosphinamide moieties instead of sulfonamides, showed similar pH-dependent relaxivities, although at other pH values owing to different pK_a values of the protonated donor sites.[20–22]

Along these lines, we reasoned that DO3A-SA ligands with additional functional groups for conjugation should be highly useful building blocks, allowing for facile inclusion of a pH-responsive MRI-CA functionality into larger constructs, such as bioconjugates or nanoparticles. We therefore synthesized and evaluated two respective ligands, featuring additional carboxylic acid moieties not intended to support metal

ion complexation. Surprisingly, the corresponding Ln^{III} complexes exhibited completely different profiles of pH-dependent relaxivity compared to those of the parent ligand, pointing at a remarkable influence of the distant functional groups, which we therefore elucidated in detail.

Results and discussion

In the following, ligands and complexes are sometimes denoted without indicating charges, protonation states, and coordinated water molecules. In these cases, it is referred to any possible species, owing to the fact that complexes with unknown or hypothetical composition are to be discussed.

Synthesis of ligands and Ln^{III}-complexes

The ligands DO3A-SA-COOH (**5**) and DO3A-SA-$(CH_2)_2$-COOH (**7**) were synthesized following a procedure adapted from the literature (Scheme 1).[23] Briefly, the secondary amine of DO3A(*t*Bu)$_3$ was functionalised with *N*-Cbz-bromoethylamine in the presence of potassium carbonate in almost quantitative yield. The carboxybenzyl protecting group was removed by hydrogenolysis and the resulting primary amine reacted with either *p*-chlorosulfonyldihydrocinnamic acid or 4-(chlorosulfonyl)benzoic acid. Removal of the *tert*-butyl protecting groups yielded the ligands **5** and **7**.

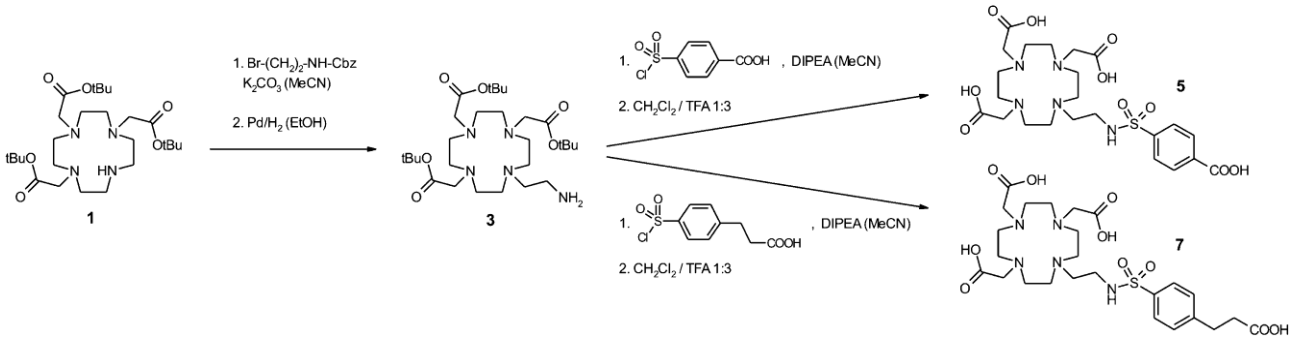

Scheme 1. Synthesis of ethylene(arylsulfonamide)-pendant DO3A ligands with peripheral carboxylic acids for conjugation.

Since complexation kinetics were reported to be slow,[16] Ln^{III} complexation was done in water at pH 6.5 and r.t. for three days. Excess Ln^{III} was removed by precipitation at pH 10, followed by centrifugation and recovery of the soluble complexes.

pH-Dependent modulation of relaxivities

The Gd^{III} complexes of **5** and **7** showed the same relaxivity, r_1 = 6.7 mM^{-1} s^{-1} at 298 K, 20 MHz and pH 7.0, which is 60% and 12% higher than that of GdDOTA and GdDO3A (r_1 = 4.2 and 6.0 mM^{-1} s^{-1}, respectively, measured at the same experimental conditions).[24] pH-Dependency of relaxivities was determined for dilute aqueous solutions over the range of pH 2 to 12. We expected that owing to a similar mechanism of deprotonation and Gd^{III} coordination of the sulfonamide associated with higher pH, a relaxivity shift should be observed for Gd-**5** and Gd-**7** around neutral pH, just like for the Gd^{III} complex of the parent ligand DO3A-SA. In addition, we reasoned that for Gd-**5** and Gd-**7**, the pH value could furthermore affect the water exchange rate τ_M and the rotational correlation time τ_R due to a change in protonation state and hydrogen bonding properties of the distant carboxylate, resulting in an additional, minor pH-dependent modulation of r_1.

However, we were surprised that the relaxivities of Gd-**5** and Gd-**7** remained virtually constant between pH 4 and 10 (see Fig. 1), particularly because it was confirmed earlier that the sulfonamides in arylsulfonamide-based GdDO3A-SA systems invariantly exhibit pK_a values around 7, while being influenced only moderately by aromatic *p*-substituents.[14,15] Typically, an off-ligation of the sulfonamide pendant arm at acidic pH results in a bis-hydrated GdDO3A-like complex ($q \sim 2$) with r_1 values above 7–8 $mM^{-1}\ s^{-1}$, while at pH > 7, deprotonation of the sulfonamide and subsequent coordination to the metal centre yields r_1 values characteristic for $q = 0$ (2–2.5 $mM^{-1}\ s^{-1}$).[15] Instead, Gd-**5** and Gd-**7** showed a peculiar behavior (Fig. 1), indicating that the sulfonamide might not be coordinated to the metal center between pH 4 and 9.

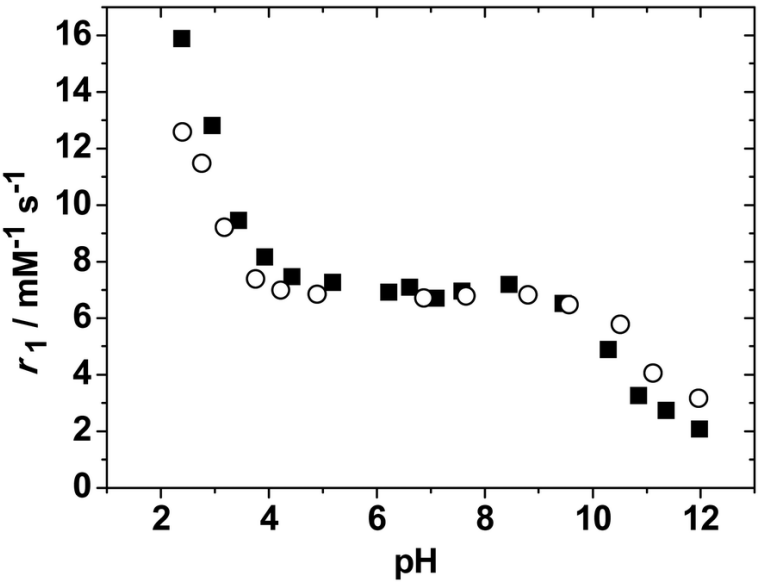

Fig. 1. pH dependent relaxivities (r_1) of Gd-**5** (circles) and Gd-**7** (squares). Data were recorded at 21 MHz and 298 K.

Furthermore, a ~50% decrease in r_1 between pH 10 and 12 was observed. Such behaviour is usually not displayed by responsive CAs based on sulfonamides. In this context, it has been reported earlier that the pK_a values of arylsulfonamides range between 10 and 12 unless located in close proximity to a strongly lewis-acidic metal centre like Zn^{II}, whereupon pK_a is lowered to values around 7.[25,26] Hence, in case the sulfonamides in Gd-**5** and Gd-**7** are kept at distance of the Gd^{III} centre, their pK_a should indeed remain around 10. Once deprotonated, Gd^{III} coordination ultimately occurs, resulting in the expected monomeric complexes with $q = 0$ and the corresponding typical r_1 values around 2. Apart from that, the observed increase of r_1 below pH 4 is fully in line with expectations, caused by protonation of the primary carboxylate donors and subsequent dissociation of the complex.[27]

Based on these observations, we assume that the Gd-**5** and Gd-**7** species feature a Gd^{III} centre coordinated to four carboxylate donors, including the carboxylates of the aromatic *p*-substituents, and a distant sulfonamide which replaces the peripheral carboxylate upon deprotonation at pH > 10. While this rationale explains the observed phenomena in terms of relaxivities, the structure of the postulated species remains unclear. Considering the steric situation, it appeared unlikely that these complexes could be monomers, pointing at presence of L_mM_n aggregates in solution. It is worth to note that the dependence of R_1 with the concentration of Gd-**7** (from 1.7 to 0.2 mM, see ESI, Fig. S1) is linear, highlighting that these aggregates are formed already at very low concentrations. Finally, they are also stable in presence of phosphate buffer at 10 mM concentration, which does not influence the measured r_1 value.

Luminescence measurements

In order to determine the hydration number and obtain further insight into the metal coordination environment, the emission spectra and lifetimes of 1 mM H_2O and D_2O solutions of [EuDO3A-SA-$(CH_2)_2$-COO]$^-$ (Eu-**7**) were recorded. A sizeable emission was observed by direct excitation of the $^5L_6 \rightarrow {}^7F_0$ transition of Eu^{III} at 395 nm.[28] The emission spectrum displays the typical $^5D_0 \rightarrow {}^7F_J$ transitions of Eu^{III} (J = 0–4, see Fig. 2). The shape of the $^5D_0 \rightarrow {}^7F_J$ emission bands is similar to those reported for the complex of DOTA and related systems.[29] We however noticed a higher $\Delta J = 2/\Delta J = 1$ intensity ratio with respect to DOTA derivatives showing C_4 symmetry, which can be attributed to a lower degree of symmetry of the Eu^{III} coordination environment in Eu-**7**. The $^5D_0 \rightarrow {}^7F_1$ transition presents three components with splittings of 126 and 223 cm^{-1} with respect to the highest energy component, caused either by low local symmetry of the Eu^{III} site or by presence of two isomers in solution (*i.e.*, SAP and TSAP conformers of DOTA-like complexes).[30]

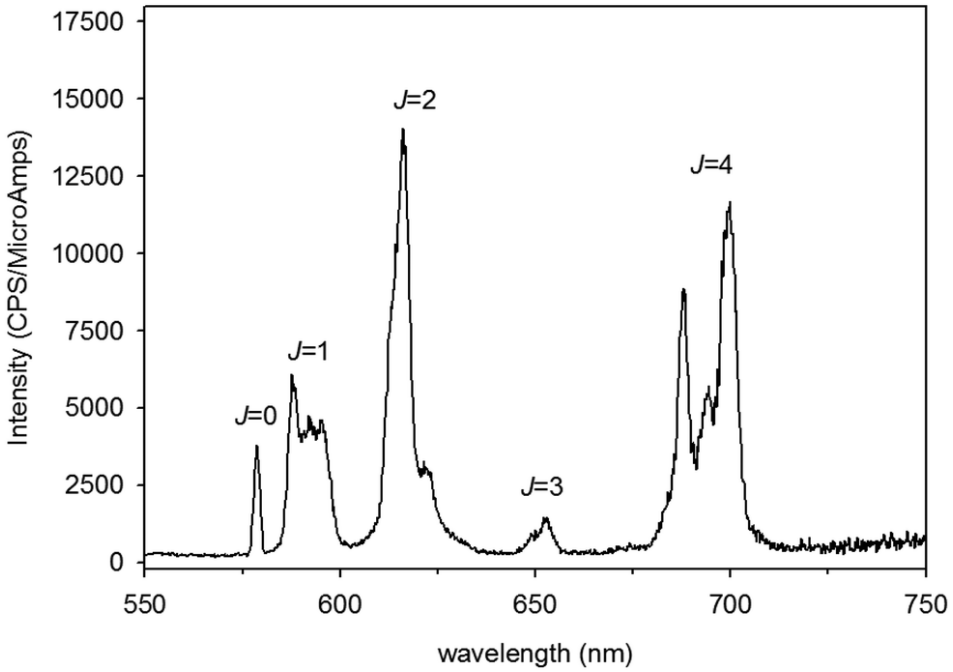

Fig. 2. Emission spectrum of the Eu-**7** complex, recorded for a 1 mM solution under excitation at 395 nm (pH = 7.2).

Lifetimes of the $^5D_0$ excited states of Eu^{III} were measured in solutions of the complexes in H_2O and D_2O to assess the hydration number of the complex. The determined values, τ_{H2O} = 0.54 ms and τ_{D2O} = 2.02 ms, correspond to hydration numbers (q) of 1.3 or 1.2, calculated according to the methods of Parker[31] and Horrocks,[32] respectively. These values indicate presence of a single water molecule in the first coordination sphere of Eu^{III}, which is in line with the observed relaxivities as well as ^1H NMRD and ^{17}O NMR data (see below). Further evidence is given by an intermediate emission lifetime recorded in H_2O (0.54 ms), being longer than those reported for pH-responsive DO3A-sulfonamides at low pH (typically 0.42–0.45 ms, corresponding to q = 2) and shorter than those measured at high pH (typically 0.7–0.9 ms, corresponding to q = 0).[14,15] The emission lifetime recorded in H_2O solution remains constant (0.54 ms) in the concentration range 1.6×10^{-5}–1.0×10^{-3} M, suggesting that the aggregates are stable in this concentration range.

Relaxometric measurements

Frequency-dependent relaxivities, that is, Nuclear Magnetic Relaxation Dispersion (NMRD) profiles, of Gd-**5** and Gd-**7** were determined for proton larmor frequencies ranging from 0.01 to 70 MHz ($B = 2.34 \times 10^{-4}$ – 1.64 T). These provide additional structural information because amplitude and shape of NMRD profiles are determined by contributions of inner-sphere (IS) and outer-sphere (OS) water to r_1. The IS term is determined by q, the water exchange rate $k_{ex} = 1/\tau_M$, τ_R, and the electronic relaxation times ($T_{1,2e}$) of Gd^{3+}. The OS term depends on $T_{1,2e}$, the relative diffusion coefficient between the complex and the water molecules (D), and their distance of closest approach, a. Since relaxivities of Gd-**5** and Gd-**7** are pH-independent between pH 4 and 10 (see above), NMRD profiles were measured for 298 K and neutral pH (Fig. 3). Almost identical datasets were obtained, resembling those of typical monohydrated low molecular weight CAs.[33] A plateau region at low field strength is followed by a single dispersion at approx. 4–8 MHz.

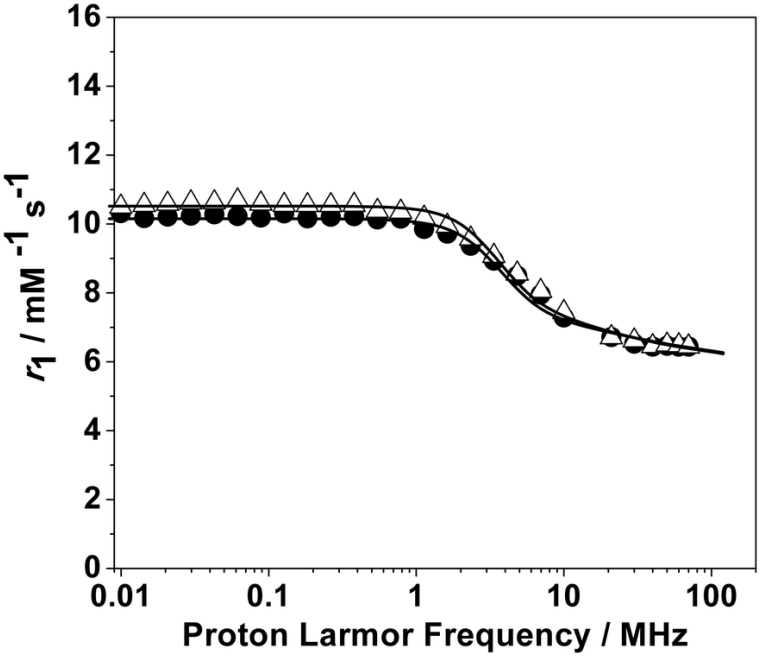

Fig. 3. ^{1}H NMRD profiles of Gd-**5** (solid circles) and Gd-**7** (open triangles). Data were recorded at 298 K and pH 6.8 and 6.7, respectively. The solid lines represent the best fitting results of the experimental data points with the parameters in Table 1.

More accurate and quantitative information on the kinetics of water exchange were obtained by measuring the temperature dependency of the solvent ^{17}O NMR reduced transverse relaxation rates $\ln(1/T_{2r})$ and shifts $\Delta\omega_r$ at 11.75 T for a 21.4 mM solution of Gd-**7** at neutral pH (Fig. 4). Temperature dependency of $1/T_{2r}$ data provides evidence for a fast water-exchange regime over the entire temperature range, while that of the reduced chemical shifts ($\Delta\omega_r$) is in line with $1/T_{2r}$ data. An increase of $1/T_{2r}$ with decreasing temperature indicates a faster water exchange rate ($1/\tau_M$) compared to Gd-DTPA or Gd-DOTA.[34] While the respective curves for these complexes show a maximum at 315 K, the maximum for Gd-**7** is observed at 280 K or below. Further evidence for fast IS water exchange dynamics is obtained from the NMRD profiles of Gd-**7** at three different temperatures (Fig. 5). For any given proton Larmor frequency, r_1 values consistently decrease with rising temperature. In particular, r_1 at 20 MHz and neutral pH decreases from 9.0 mM^{-1} s^{-1} to 5.0 mM^{-1} s^{-1} at 283 K and 310 K, respectively. This behaviour is characteristic for small chelates, bearing a coordinated water molecule in fast exchange with the bulk, and a τ_M short enough not to limit the relaxivity.

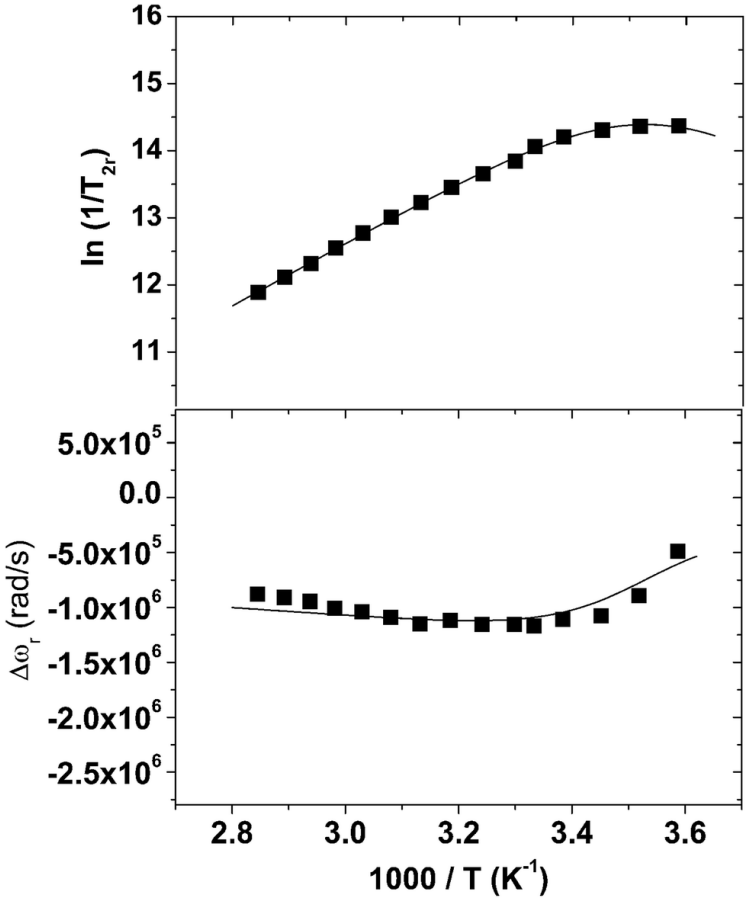

Fig. 4. Reduced transverse ^{17}O relaxation rates (above) and chemical shifts (below) measured at 11.74 T (pH 6.6) for Gd-**7**. The solid lines correspond to the fits of the data as described in the text.

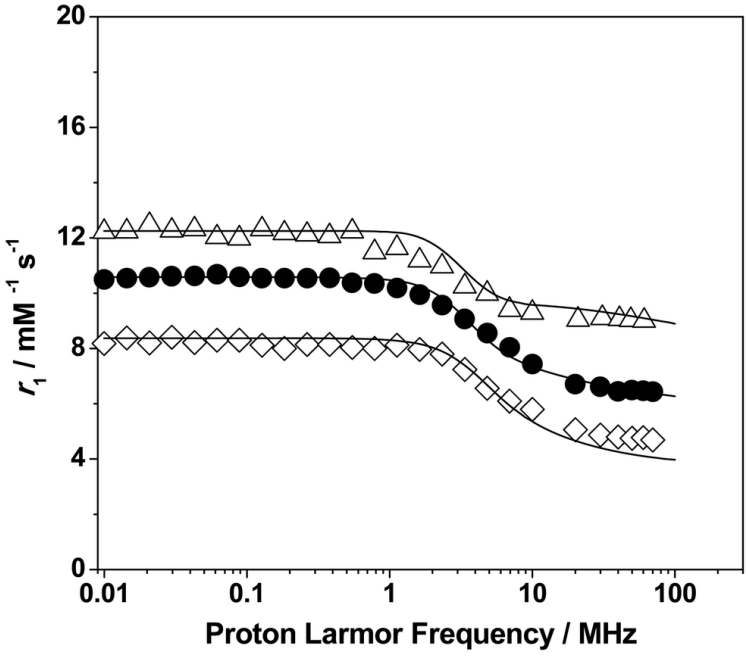

Fig. 5. ^{1}H NMRD profiles of Gd-**7** at 283 K (open triangles), 298 K (solid circles) and 310 K (open diamonds) (pH 6.66).

The experimental data, ^{1}H NMRD and ^{17}O NMR, were fitted simultaneously, according to the established theory of paramagnetic relaxation, expressed by the Solomon–Bloembergen–Morgan (SBM)[35] and Freed's[36] equations for the inner- and outer-sphere proton relaxation mechanisms, respectively, and of the Swift–Connick theory for ^{17}O relaxation.[37] The ^{17}O R_2 data depend on a series of parameters such as $T_{1,2e}$, the hyperfine Gd–$^{17}O_{water}$ coupling constant $A_O/\hbar$, τ_M, and q. Information on q and $A_O/\hbar$ are derived from the temperature dependence of $\Delta\omega$. Additional relevant parameters are those associated with the electronic relaxation times $T_{1,2e}$, that is, the trace of the square of the zero-field splitting tensor, Δ^2; the correlation time describing the modulation of the zero-field splitting, τ_V, and its activation energy, E_V; the enthalpy of activation for the water exchange process, $\Delta H^{\#}_M$. The data fitting was optimized by using fixed values for some of the relaxation parameters: q = 1, a = 4.0 Å, ^{298}D = 2.24 × 10^{-5} cm^2 s^{-1}, the distance between the metal ion and the protons of the bound water molecule, r_{GdH} = 3.1 Å.

A good fit was obtained and the resulting structural and dynamic molecular parameters describing the magnetic interaction of the solvent nuclei and the metal center are listed in Table 1. In particular, the residence lifetime of the bound water molecule was confirmed to be as short as 40 ns ($^{298}k_{ex}$ = 25 × 10^6 s^{-1}). It is reasonable to assume a similar value for the other parent chelate, Gd-**5**. Notably, a reorientational correlation time of 145 ps was calculated for both complexes, which is much longer than that observed for monomeric Gd^{III}-chelates with similar molecular weight. In particular, GdDO3A-SA bearing a methoxyphenyl group, a complex with similar molecular weight to Gd-**5** and Gd-**7**, showed a τ_R of 94 ps.[18] In order to illustrate the implications of this result, Table 1 also lists the relaxometric parameters for GdDOTA and $Gd_2Pip(DO3A)_2$, a dimeric Gd^{III} complex featuring two DOTA-monoamide units linked by a piperidine heterocycle.[34] The monomer GdDOTA and the dimeric complex exhibit τ_R of 77 ps and 171 ps, respectively, the latter value being more similar to that of Gd-**5** and Gd-**7**, pointing at a dimeric structure for these species. The higher τ_R value is furthermore in good accordance with a broad hump of r_1 between 20 and 70 MHz shown by the NMRD profile of Gd-**7** at 283 K, pointing at low rotational dynamics of this species. From a fit to this NMRD profile, a τ_R value of 210 ps is obtained for T = 283 K, supporting the notion of presence a dimer. In order to further confirm the correctness of the analysis, we performed the fitting also using q = 2 and a best-fit was obtained only using a τ_R value of 68 ps, lower than the value obtained for GdDOTA (see ESI, Fig. S2).

Table 1. Best-fit parameters obtained from the analysis of the $1/T_1$ ^{1}H NMRD profiles collected at 298 K and ^{17}O NMR data.

Parameter	Gd-7	Gd-5	$Gd_2Pip(DO3A)_2$	GdDOTA
$^{298}\tau_M$/ns	40 ± 8	40	667	244
$\Delta H^{\#}_M$/kJ mol^{-1}	42.3 ± 1.2	—	34.2	49.8
$A/\hbar/10^6$ rad s^{-1}	−3.1 ± 0.1	—	−3.7	−3.8
$^{298}\tau_R$/ps	145.6 ± 2.2	145.1 ± 2.0	171	77
$^{298}\tau_V$/ps	44.5 ± 2.4	43.2 ± 2.2	19	11
$\Delta^2/10^{19}$ s^{-2}	1.53 ± 0.11	1.71 ± 0.10	1.7	1.6

The outer sphere contribution to relaxivity was estimated by using standard values for the distance of closest approach, a (4 Å).

Hypothetical structures

In summary, the relaxometric data strongly suggest that at neutral pH, Gd-**5** and Gd-**7** are actually forming dimeric structures, $[Gd_2(\mathbf{5})_2]$ and $[Gd_2(\mathbf{7})_2]$. As indicated above, the observed pH dependency profile of r_1 allows for the conclusion that between pH 4 and 10, dimerisation occurs *via* coordination of the peripheral carboxylate of one complex monomer with the metal centre of another one, while the sulfonamide is not involved in Gd^{III} coordination. These species are apparently of remarkable stability because they are invariantly present under conditions typically promoting formation of monomers, that is, at low Gd^{III} concentration (<0.5 mM) or in 10 mM phosphate buffer.

As a further argument in favour of dimerization, a linear graph of τ_R*versus* molecular weight comparing $[Gd_2(\mathbf{5})_2]$ and $[Gd_2(\mathbf{7})_2]$ with other examples of monomeric and dimeric Gd-complexes is shown in Fig. 6. Our hypothesis is in line with previous studies, showing that carboxylate units can mediate the formation of stable trinuclear La^{III} entities in aqueous solution[40] as well as the aggregation of dinuclear Gd^{III} complexes with DO3A ligands linked by rigid spacers.[41,42] Finally, our Eu^{III} luminescence measurements indicated presence of one Eu^{III}-bound water per metal centre in Eu-**7**, which is also in line with the observed relaxivities and NMRD profiles. However, it should be noted that GdDO3A-SA derivatives reported by Lowe *et al.*[15] contain three peripheral carboxylate groups that could, in principle, also interact with the Gd-centre of another monomeric unit and form aggregates, thus preventing a pH-dependent relaxivity. Actually, in that case, aggregation did not occur and pH-dependency was maintained; we presume that the shorter length of the spacer with respect to the one present in case of Gd-**5** and Gd-**7** may have prevented dimerization.

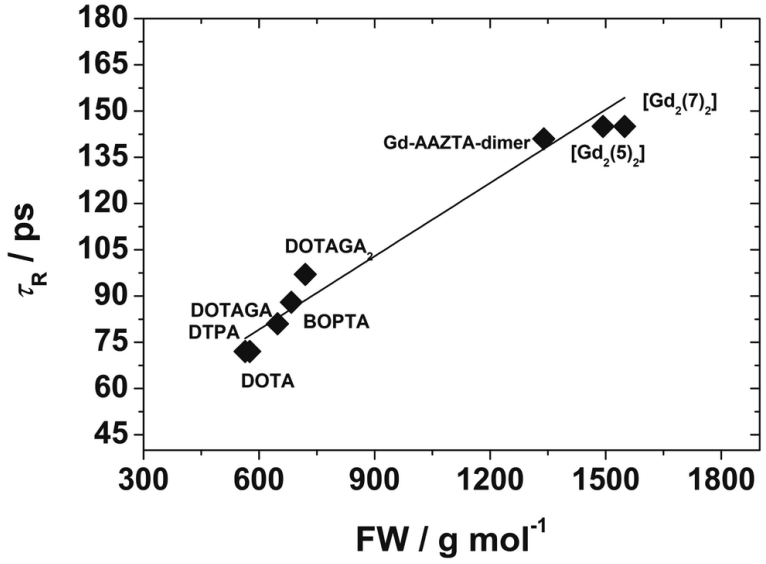

Fig. 6. Plot of the rotational correlation times of selected polyaminocarboxylate Gd-complexes as a function of molecular weight. The correlation coefficient *R* of the best fit line is 0.99. Data taken from ref. 24, 38 and 39 and this work.

To gain additional insight into the structure of the complexes in solution, we recorded the ^{1}H NMR spectrum of Eu-**7** (see ESI, Fig. S3). Unfortunately, the spectrum shows broad featureless signals likely related to exchange processes present in solution. This may be related to the presence of aggregates in solution and/or to the exchange between SAP and TSAP isomers. One can notice very broad signals in the range 25–30 ppm that are characteristic of the most shifted signals of the SAP isomer.

Finally, we recorded the ^{1}H DOSY NMR spectrum (500 MHz, D_2O) of diamagnetic analogues La-**5**, and compared the results to LaDTPA (see ESI, Fig. S4). The spectrum of La-**5** shows very broad signals owing to presence of dimers, similar to observations made for Eu-**7**. The different translational diffusion coefficients (*D*) of the two compounds, $(2.2 \pm 0.2) \times 10^{-10}$ m^2 s^{-1} for La-**5** and $(3.80 \pm 0.65) \times 10^{-10}$ m^2 s^{-1} for LaDTPA can be ascribed to the different molecular weight, thus strongly supporting the notion of presence of La-**5** in a dimeric form.

Altogether, our solution data provide strong evidence for a composition of $[Gd_2(\mathbf{L})_2(H_2O)_2]$ for complexes of both ligands (**L** = **5** or **7**), while it is most reasonable to assume symmetrical structures with bridging ligands **L** and one metal-bound water per Gd^{III}. Based on this presumption, possible geometries for both species were elucidated by means of density functional theory (DFT) calculations.

DFT-calculated structures

Geometry optimisations of the $[Gd_2(\mathbf{L})_2(H_2O)_2]$ systems provided energy minima that correspond to the well-known square-antiprismatic (SAP) and twisted-square antiprismatic (TSAP) isomers of DOTA-like complexes (Fig. 7). As expected, the lower plane of the coordination polyhedron is defined by the four nitrogen atoms of the macrocycle, while the upper plane is delineated by three oxygen atoms of the acetate groups and one oxygen atom of the carboxylate group of the sulfonamide arms. The calculated Gd–O distances involving the carboxylate group of the sulfonamide pendant fall within the range 2.45–2.52 Å, being somewhat longer than the distances between the metal ion and the oxygen atoms of acetate groups (2.36–2.42 Å).

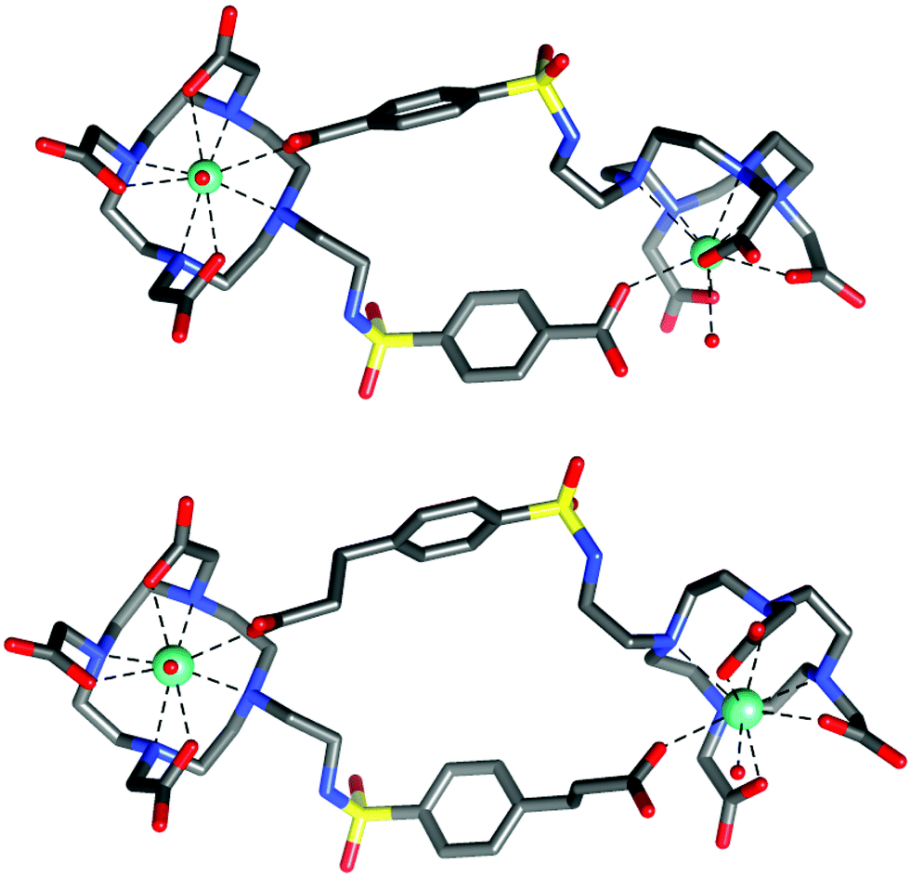

Fig. 7. Geometries of the TSAP conformers of $[Gd_2(\mathbf{5})_2(H_2O)_2]$ (top) and $[Gd_2(\mathbf{7})_2(H_2O)_2]$ (bottom), obtained from DFT calculations at the TPSSh/LCRECP/6-31G(d) level. For the corresponding SAP conformers see the ESI, Fig. S1.

The relative free energies of the TSAP and SAP isomers favor the TSAP forms of $[Gd_2(\mathbf{7})_2(H_2O)_2]$ by only 0.26 kcal mol^{-1}, while for $[Gd_2(\mathbf{5})_2(H_2O)_2]$, the two isomers exhibit virtually identical free energies. Thus, we assume that two diastereoisomers are present in solution, slightly favoring the TSAP isomer. Since the latter type of conformer is generally characterized by water exchange rates that are about one order of magnitude higher than those of the corresponding SAP forms, the fast exchange determined by the analysis of the ^1H NMRD and ^{17}O NMR data is well explained, which furthermore corresponds to the coordination of the carboxylate group of the sulfonamide arm on the O_4 plane of the coordination polyhedron, leaving the coordinated water molecule at the labile capping position.[43] Due to the different length of the aromatic substituents, varying Gd–Gd distances of 13.8 and 15.3 Å are found for $[Gd_2(\mathbf{5})_2(H_2O)_2]$ and $[Gd_2(\mathbf{7})_2(H_2O)_2]$, respectively.

Conclusion

In order to obtain building blocks for inclusion of a pH-dependent MRI contrast agent functionality into larger constructs, such as bioconjugates, nanoparticles, or micelles, we synthesised derivatives of the established pH-responsive CA motif Gd(DO3A-SA), bearing additional carboxylic acid moieties on the sulfonamide-pendant arm of the DO3A backbone. Our findings illustrate that such a seemingly innocent, peripheral functionalisation of these pH-responsive MRI-CA actually has a dramatic influence on the complex structure in solution, essentially resulting in a complete loss of pH-dependency of relaxivity in the biologically relevant pH range (4 to 9). Despite the steric position of the anchor groups was designed not to interfere with the Gd^{III} coordination environment, experimental evidence supports the hypothesis of dimer formation involving the distant carboxylates, thus preventing Gd^{III}-coordination of the deprotonated sulfonamide at neutral pH. Most notably, these dimers are very stable even at low concentrations and in presence of coordinating anions such as phosphate, and exhibit larger relaxivities than comparable GdDOTA- or GdDO3A-monomers, owing to larger rotational correlation times and a favorable ratio of square-antiprismatic and twisted square-antiprismatic conformers of the Gd^{III} coordination environment. Hence, such ligands, resulting in dimeric or multimeric Gd^{III} complexes, might inspire future design of high-relaxivity Gd^{III}-based MRI-CA by exploiting formation of supramolecular structures by self-assembly. Notwithstanding this, dimerisation is unlikely to occur after further functionalisation on the peripheral carboxylates, resulting in non-coordinating or bulky moieties at this position. Hence, our ligands are nonetheless to be considered suitable for the initially intended purpose, warranting further application in this context.

Experimental

Materials and methods

^1H NMR spectra were recorded on a Bruker AV400 at 298 K and a Bruker AV500cr equipped with a cryogenic probe. ^1H NMR DOSY spectra were recorded on a Bruker Avance III spectrometer operating at 11.7 T. HPLC analyses were done using a Nucleosil 100-5C18 (125 × 4.6 mm, CS Chromatographie) column on a Shimadzu HPLC System, equipped with a two-channel UV-VIS detector. For identification of the compounds absorbances at 214 nm and 254 nm were recorded. Mass spectra were recorded on a Varian 500-MS IT Mass Spectrometer. All synthesised compounds were purified on a J'Sphere ODS-H80 column (150 × 20 mm, YMC HPLC Column) using either a Sykam S 1121 HPLC System equipped with a DAD detector (Sykam S3210 UV/VIS Detector) or a semipreparative Shimadzu LC-20AT HPLC System, equipped with a SPD-20A UV-VIS detector. Solvents for analytical and preparative HPLC runs were H_2O with 0.1% trifluoroacetoc acid (TFA) (A) and MeCN with 0.1% TFA (B). Analytical runs to characterize the

Gd^{III} complexes were done using solvents without the addition of TFA. Chemicals and solvents (HPLC grade) were purchased from various commercial suppliers and used as received.

Ligand syntheses

DO3A(*t*Bu)$_3$-(CH$_2$)$_2$-NH-Cbz (2). DO3A(*t*Bu)$_3$ (**1**, 1.00 g, 1.94 mmol) was dissolved in 20 mL dry MeCN and K_2CO_3 (806 mg, 5.83 mmol) was added. *N*-Cbz-Bromoethylamine (501 mg, 1.94 mmol) was dissolved in 5 mL dry MeCN and added dropwise over 1 h. The resulting solution was stirred at room temperature overnight. The crude product was purified by HPLC (30–68% B in 10 min, flow rate 10 mL min^{-1}, elution time = 7.5 min). The collected fractions were lyophilized and the product obtained as a white solid as the mono-trifluoroacetate salt (1.4 g, 1.74 mmol, 89.6%). Analytical HPLC (20–100% B in 15 min): t_R = 9.9 min. MS (ESI$^+$): $C_{36}H_{62}N_5O_8$ *m/z*: calcd 692.9 $[M + H]^+$; found 692.8 $[M + H]^+$, 714.7 $[M + Na]^+$.

DO3A(*t*Bu)$_3$-(CH$_2$)$_2$-NH$_2$ (3). Under nitrogen atmosphere, **2** (1.40 g, 1.74 mmol) was dissolved in 60 mL EtOH and Pd/C (140 mg, 10 wt%) was added. The flask was saturated with hydrogen and the suspension stirred at room temperature overnight. The crude product was purified over Celite 545 (particle size 0.01–0.04 mm, preconditioning and elution with MeOH). The product was obtained as a colourless, highly viscous liquid (0.94 g, 1.68 mmol, 96.5%). Analytical HPLC (10–100% B in 15 min): t_R = 6.8 min. MS (ESI$^+$): $C_{28}H_{56}N_5O_6$ *m/z*: calcd 558.8 $[M + H]^+$; found 558.8 $[M + H]^+$, 580.7 $[M + Na]^+$; ^{1}H NMR (400 MHz, 298 K, DMSO-d$_6$): δ (ppm) = 1.42–1.45 (m, 27 H), 2.89–3.46 (m, 20 H), 3.5–3.77 (m, 6 H), 8.28 (bs, 2 H).

DO3A(*t*Bu)$_3$-SA-(CH$_2$)$_2$-COOH (6). 3 (100 mg, 179 µmol) was dissolved in 3 mL dry MeCN. DIPEA (116 mg, 156 µL, 896 µmol) was added and the solution cooled on ice. *p*-Chlorosulfonyldihydrocinnamic acid (45 mg, 179 µmol) was dissolved in 1 mL dry MeCN and added dropwise over 1 h. The resulting solution was slowly warmed to room temperature and stirred overnight. The reaction was quenched by addition of 2 mL H_2O and the product purified by HPLC (25–55% in 10 min, t_R = 8.9 min). The product was obtained as a colourless solid (50 mg, 65 µmol, 36.2%). Analytical HPLC (10–100% B in 15 min): t_R = 8.2 min. MS (ESI$^+$): $C_{37}H_{64}N_5O_{10}S$ *m/z*: calcd 770.0 $[M + H]^+$; found 770.8 $[M + H]^+$, 792.6 $[M + Na]^+$; ^{1}H NMR (400 MHz, 298 K, DMSO-d$_6$): δ (ppm) = 1.35–1.42 (m, 18 H), 1.44–1.50 (m, 9 H), 2.41 (t, 2 H, $^3J_{HH}$ = 7.0 Hz), 2.82 (t, 2 H, $^3J_{HH}$ = 7.0 Hz), 2.86–3.18 (m, 12 H), 3.32–3.44 (m, 8 H), 3.45–3.61 (m, 6 H), 7.14 (d, 2 H, $^3J_{HH}$ = 8.2 Hz), 7.50 (d, 2 H, $^3J_{HH}$ = 8.2 Hz), 8.09 (t, 1 H, $^3J_{HH}$ = 5.3 Hz).

DO3A-SA-(CH$_2$)$_2$-COOH (7). *tert*-Butyl protecting groups of **6** (50 mg, 65 µmol) were removed by reaction with 2 mL DCM/TFA (1 : 3) overnight. Then, the solvent was removed under a stream of nitrogen and the crude product purified by HPLC (3–20% in 10 min, t_R = 4–6 min). The product was obtained as a colourless solid (27 mg, 45 µmol, 69.4%). Analytical HPLC (3–20% B in 15 min): t_R = 5.3 min. MS (ESI$^+$): $C_{25}H_{40}N_5O_{10}S$ *m/z*: calcd 602.7 $[M + H]^+$; found 602.6 $[M + H]^+$, 624.4 $[M + Na]^+$.

DO3A(*t*Bu)$_3$-SA-COOH (4). 3 (300 mg, 539 µmol) was dissolved in 5 mL dry MeCN. DIPEA (348 mg, 469 µL, 2.69 mmol) was added and the solution cooled on ice. 4-(Chlorosulfonyl)benzoic acid (119 mg, 539 µmol) was dissolved in 2 mL dry MeCN and added dropwise over 1.5 h. The resulting solution was slowly warmed to room temperature and stirred overnight. The reaction was quenched by addition of 2 mL H_2O and the product purified by HPLC (30–50% in 10 min, t_R = 7.2 min). The product was obtained as a colourless solid (73.5 mg, 99.1 µmol, 18.4%). Analytical HPLC (10–100% B in 15 min): t_R = 7.9 min. MS (ESI$^+$): $C_{35}H_{60}N_5O_{10}S$ *m/z*: calcd 742.9 $[M + H]^+$; found 742.9 $[M + H]^+$, 764.6 $[M + Na]^+$; ^{1}H NMR (400 MHz, 298 K, DMSO-d$_6$): δ (ppm) = 1.36–1.42 (m, 18 H), 1.47–1.52 (m, 9 H), 2.86–3.13 (m, 10 H), 3.34–3.56 (m, 16 H), 7.68 (d, 2 H, $^3J_{HH}$ = 8.2 Hz), 7.82 (d, 2 H, $^3J_{HH}$ = 8.2 Hz), 8.82–8.86 (m, 1 H).

DO3A-SA-COOH (5). *tert*-Butyl protecting groups of **4** (74 mg, 99 µmol) were removed by reaction with 2 mL DCM/TFA (1 : 3) overnight. The crude product was precipitated in Et_2O and purified by HPLC (3–20% in 10 min, t_R = 3–6 min). The product was obtained as a colourless solid (47 mg, 83 µmol, 83.4%).

Analytical HPLC (3–20% B in 15 min): t_R = 3.7 min. MS (ESI^+): $C_{23}H_{36}N_5O_{10}S$ *m/z*: calcd 574.6 $[M + H]^+$; found 574.8 $[M + H]^+$, 596.7 $[M + Na]^+$.

Synthesis of the Ln^{III}-complexes

The two ligands were dissolved at *ca.* 25 mM concentration in Tracepur® water. Gd, Eu or La-chloride hexahydrate (0.5 M aqueous solutions) was added in a slight excess (1.1 eq.). The pH was gradually adjusted to 6.5 and the solution stirred at room temperature for three days. The pH was then increased to 10 to precipitate excess Ln^{III} as hydroxide. The solution was centrifuged (3000 rpm, 3 min, r.t.) and the supernatant filtered through a 0.2 μm filter. The pH was re-adjusted to 7 and the solvent removed *in vacuo*. The Ln^{III}-complexes were isolated as colourless solids in quantitative yields.

Gd-**7**: Analytical HPLC (3–20% B in 15 min): t_R = 3.6 min. MS (ESI^+): $C_{25}H_{36}GdN_5O_{10}S$ *m/z*: calcd 756.0 $[M + H]^+$; found 756.3 $[M + H]^+$, 779.3 $[M + Na]^+$.

Eu-**7**: MS (ESI^+): $C_{25}H_{36}EuN_5O_{10}S$ *m/z*: calcd 750.6 $[M + H]^+$; found 750.3 $[M + H]^+$, 773.3 $[M + Na]^+$.

Gd-**5**: Analytical HPLC (3–20% B in 15 min): t_R = 3.7 min. MS (ESI^+): $C_{23}H_{31}GdN_5O_{10}S$ *m/z*: calcd 727.8 $[M + H]^+$; found 728.4 $[M + H]^+$, 750.3 $[M + Na]^+$.

La-**5**: Analytical HPLC (3 min at 0% B, then 0–100% B in 15 min): t_R = 9.7 min. MS (ESI^+): $C_{23}H_{31}LaN_5O_{10}S$ *m/z*: calcd 709.5 $[M + H]^+$; found 709.4 $[M + H]^+$.

^{1}H NMR relaxometric measurements

^{1}H NMRD profiles were recorded using a fast-field-cycling Stelar SmarTracer relaxometer at magnetic field strengths between 0.00024 and 0.25 T (which correspond to 0.01–10 MHz proton Larmor frequencies). The relaxometer operated under computer control with an absolute uncertainty in $1/T_1$ of ±1%. Additional data points in the range of 20–70 MHz were obtained using a Stelar Relaxometer and a Bruker WP80 NMR electromagnet adapted to variable-field measurements (20–70 MHz proton Larmor frequency). ^{1}H T_1 relaxation times at high magnetic fields were acquired with an inversion recovery experiment with a mean 90° pulse width of 3.5 μs. The pH dependent relaxivities were measured at 20 MHz, 298 K in aqueous solution. pH values were adjusted by addition of 0.1 M NaOH and 0.1 M HCl, respectively. ^{17}O NMR measurements were recorded on a Bruker Avance III spectrometer (11.7 T) equipped with a 5 mm probe. The analysis was carried out using a Gd^{III} complex solution of approx. 20 mM concentration, containing 2.0% of the ^{17}O isotope. The exact Gd^{III} concentrations were determined accordingly to Corsi *et al.* from the lanthanide(iii)-induced shift of the *tert*-BuOH signal.[44]

Luminescence measurements

Emission and excitation spectra were measured on a Horiba FluoroMax Plus-P spectrofluorometer equipped with a 150 W ozone-free xenon arc lamp and a R928P photon counting emission detector, as well as a photodiode reference detector for monitoring lamp output. Luminescence decays were measured on the same instrument working in the phosphorescence mode using a xenon flash lamp.

Density functional theory (DFT) calculations

All calculations were carried out using the TPSSh exchange–correlation functional,[45] which belongs to the hybrid meta-GGA family, and the Gaussian 09 package (Revision D.01).[46] Geometry optimizations of the $[Gd_2(\mathbf{L})_2(H_2O)]_2$ systems were performed using the large-core relativistic effective core potential (LCRECP) of Dolg *et al.*, which includes 46 + $4f^7$ electrons of Gd^{3+} in the core, and the associated (7s6p5d)/[5s4p3d]-GTO valence basis set.[47] The standard 6-31G(d) basis set was used for all other atoms. Bulk solvent effects (water) were considered with the polarizable continuum model (PCM). We selected the integral equation

formalism (IEFPCM),[48] together with universal force field radii (UFF)[49] scaled by a factor of 1.1, to define the solute cavities.

Conflicts of interest

There are no conflicts to declare.

Acknowledgements

Lorenzo Tei sincerely acknowledges the Alexander von Humboldt Foundation (AvH) for a Research fellowship. The authors also thank Dr. Claudio Cassino for the help in acquisition of ^{1}H NMR DOSY spectra, and the Deutsche Forschungsgemeinschaft (CRC 824) for support.

References

01 P. Caravan, C. T. Farrar, L. Frullano and R. Uppal, *Contrast Media Mol. Imaging*, 2009, **4**, 89−100.

02 K. R. Thulborn, J. C. Waterton, M. Matthews and G. K. Radda, *Biochim. Biophys. Acta*, 1982, **714**, 265−270.

03 L. Pauling and C. D. Coryell, *Proc. Natl. Acad. Sci. U. S. A.*, 1936, **22**, 210−216.

04 M. E. Raichle *Proc. Natl. Acad. Sci. U. S. A.*, 1998, **95**, 765−772.

05 G. Angelovski *Angew. Chem., Int. Ed.*, 2016, **55**, 7038−7046.

06 M. Carril *J. Mater. Chem. B*, 2017, **5**, 4332−4347.

07 C. T. Yang and K. H. Chuang, *MedChemComm*, 2012, **3**, 552−565.

08 (*a*) S. M. J. van Duijnhoven, M. S. Robillard, S. Langereis and H. Grüll, *Contrast Media Mol. Imaging*, 2015, **10**, 282−308. (*b*) D. V. Hingorani, A. S. Bernstein and M. D. Pagel, *Contrast Media Mol. Imaging*, 2015, **10**, 245−265. (*c*) C. Shen and E. New, *Curr. Opin. Chem. Biol.*, 2013, **17**, 158−166.

09 C. Tu, R. Nagao and A. Y. Louie, *Angew. Chem., Int. Ed.*, 2009, **48**, 6547−6551.

10 A. Razgulin, N. Ma and J. Rao, *Chem. Soc. Rev.*, 2011, **40**, 4186−4216.

11 E. L. Que and C. J. Chang, *Chem. Soc. Rev.*, 2010, **39**, 51−60.

12 S. Zhang, K. Wu and A. D. Sherry, *Angew. Chem.*, 1999, **111**, 3382−3384.

13 F. K. Kálmán, M. Woods, P. Caravan, P. Jurek, M. Spiller, G. Tircsó, R. Király, E. Brücher and A. D. Sherry, *Inorg. Chem.*, 2007, **46**, 5260−5270.

14 M. P. Lowe and D. Parker, *Chem. Commun.*, 2000, 707−708.

15 M. P. Lowe, D. Parker, O. Reany, S. Aime, M. Botta, G. Castellano, E. Gianolio and R. Pagliarin, *J. Am. Chem. Soc.*, 2001, **123**, 7601−7609.

16 A. Takács, R. Napolitano, M. Purgel, A. C. Bényei, L. Zékány, E. Brücher, I. Tóth, Z. Baranyai and S. Aime, *Inorg. Chem.*, 2014, **53**, 2858−2872.

17 L. Moriggi, M. A. Yaseen, L. Helm and P. Caravan, *Chem. – Eur. J.*, 2012, **18**, 3675−3686.

18 E. Gianolio, S. Porto, R. Napolitano, S. Baroni, G. B. Giovenzana and S. Aime, *Inorg. Chem.*, 2012, **51**, 7210−7217.

19 (*a*) R. Pal and D. Parker, *Org. Biomol. Chem.*, 2008, **6**, 1020−1033. (*b*) D. G. Smith, B. K. McMahon, R. Pal and D. Parker, *Chem. Commun.*, 2012, **48**, 8520−8522. (*c*) B. K. McMahon, R. Pal and D. Parker, *Chem. Commun.*, 2013, **49**, 5363−5365.

20 G. B. Giovenzana, R. Negri, G. A. Rolla and L. Tei, *Eur. J. Inorg. Chem.*, 2012, 2035−2039.

21 Z. Baranyai, G. A. Rolla, R. Negri, A. Forgács, G. B. Giovenzana and L. Tei, *Chem. – Eur. J.*, 2014, **20**, 2933−2944.

22 M. Giardiello, M. Botta and M. P. Lowe, *Inorg. Chem.*, 2013, **52**, 14264−14269.

23 E. Gianolio, R. Napolitano, F. Fedeli, F. Arena and S. Aime, *Chem. Commun.*, 2009, 6044−6046.

24 P. Caravan, J. J. Ellison, T. J. McMurry and R. B. Lauffer, *Chem. Rev.*, 1999, **99**, 2293−2352.

25 T. Koike, E. Kimura, I. Nakamura, Y. Hashimoto and M. Shiro, *J. Am. Chem. Soc.*, 1992, **114**, 7338−7345.

26 E. Kimura and T. Koike, *Chem. Soc. Rev.*, 1998, **27**, 179−184.

27 S. Aime, M. Botta, S. G. Crich, G. Giovenzana, R. Pagliarin, M. Sisti and E. Terreno, *Magn. Reson. Chem.*, 1998, **36**, S200−S208.

28 K. Binnemans *Coord. Chem. Rev.*, 2015, **295**, 1−45.

29 M. Woods, S. Aime, M. Botta, J. A. K. Howard, J. M. Moloney, M. Navet, D. Parker, M. Port and O. Rousseaux, *J. Am. Chem. Soc.*, 2000, **122**, 9781−9792.

30 R. S. Dickins, D. Parker, J. I. Bruce and D. J. Tozer, *Dalton Trans.*, 2003, 1264−1271.

31 A. Beeby, I. M. Clarkson, R. S. Dickins, S. Faulkner, D. Parker, L. Royle, A. S. de Sousa, J. A. G. Williams and M. Woods, *J. Chem. Soc., Perkin Trans. 2*, 1999, 493−503.

32 R. M. Supkowski and W. D. Horrocks, Jr., *Inorg. Chim. Acta*, 2002, **340**, 44−48.

33 S. Aime, M. Botta, M. Fasano and E. Terreno, *Chem. Soc. Rev.*, 1998, **27**, 19−29.

34 D. H. Powell, O. M. N. Dhubhghaill, D. Pubanz, L. Helm, Y. S. Lebedev, W. Schlaepfer and A. E. Merbach, *J. Am. Chem. Soc.*, 1996, **118**, 9333−9346.

35 N. Bloembergen and L. O. Morgan, *J. Chem. Phys.*, 1961, **34**, 842−850.

36 J. H. Freed *J. Chem. Phys.*, 1978, **68**, 4034−4037.

37 T. J. Swift and R. E. J. Connick, *J. Chem. Phys.*, 1962, **37**, 307−320.

38 F. Kielar, L. Tei, E. Terreno and M. Botta, *J. Am. Chem. Soc.*, 2010, **132**, 7836−7837.

39 L. Tei, G. Gugliotta, G. Gambino, M. Fekete and M. Botta, *Isr. J. Chem.*, 2017, **57**, 887−895.

40 A. Rodriguez-Rodriguez, Z. Garda, E. Ruscsak, D. Esteban-Gomez, A. de Blas, T. Rodriguez-Blas, L. M. P. Lima, M. Beyler, R. Tripier, G. Tircso and C. Platas-Iglesias, *Dalton Trans.*, 2015, **44**, 5017−5031.

41 J. Costa, E. Balogh, V. Turcry, R. Tripier, M. Le Baccon, F. Chuburu, H. Handel, L. Helm, E. Tóth and A. E. Merbach, *Chem. – Eur. J.*, 2006, **12**, 6841−6851.

42 M. Regueiro-Figueroa, A. Nonat, G. A. Rolla, D. Esteban-Gomez, A. de Blas, T. Rodriguez-Blas, L. J. Charbonniere, M. Botta and C. Platas-Iglesias, *Chem. – Eur. J.*, 2013, **19**, 11696−11706.

43 A. Rodriguez-Rodriguez, M. Regueiro-Figueroa, D. Esteban-Gomez, T. Rodriguez-Blas, V. Patinec, R. Tripier, G. Tircso, F. Carniato, M. Botta and C. Platas-Iglesias, *Chem. – Eur. J.*, 2017, **23**, 1110−1117.

44 D. M. Corsi, C. Platas-Iglesias, H. van Bekkum and J. A. Peters, *Magn. Reson. Chem.*, 2001, **39**, 723−726.

45 J. M. Tao, J. P. Perdew, V. N. Staroverov and G. E. Scuseria, *Phys. Rev. Lett.*, 2003, **91**, 146401.

46 M. J.Frisch, G. W.Trucks, H. B.Schlegel, G. E.Scuseria, M. A.Robb, J. R.Cheeseman, G.Scalmani, V.Barone, B.Mennucci, G. A.Petersson, *et al.*, Gaussian 09, Revision D.01, Gaussian, Inc., Wallingford CT, 2009.

47 M. Dolg, H. Stoll, A. Savin and H. Preuss, *Theor. Chim. Acta*, 1989, **75**, 173−194.

48 J. Tomasi, B. Mennucci and R. Cammi, *Chem. Rev.*, 2005, **105**, 2999−3093.

49 A. K. Rappe, C. J. Casewit, K. S. Colwell and W. A. Goddard, *J. Am. Chem. Soc.*, 1992, **114**, 10024.

[i] Electronic supplementary information (ESI) available. See DOI: 10.1039/c7dt02985c.